Environmental Science & Technology

pubs.acs.org/est

Article

# Isotope-Based Characterization of Soil Elemental Mercury Emissions from Historical Mercury Mining Areas: Driving Pathways and Relative Contributions

Qingyi Cao, Haiyan Hu, Wei Yuan, Jen-How Huang, Xuewu Fu, and Xinbin Feng*

Cite This: *Environ. Sci. Technol.* 2024, 58, 16824−16832

Read Online

ACCESS | Metrics & More | Article Recommendations | Supporting Information



**ABSTRACT:** Photo-, microbial, and abiotic dark reduction of soil mercury (Hg) may all lead to elemental mercury (Hg(0)) emissions. Utilizing lab incubations, isotope signatures of Hg(0) emitted from mining soils were characterized to quantify the interplay and contributions of various Hg reduction pathways, which have been scarcely studied. At 15 °C, microbial reduced Hg(0) showed a negative mass-dependent fractionation (MDF) ($\delta^{202}$Hg = −0.30 ± 0.08‰, 1SD) and near-zero mass-independent fractionation (MIF) ($\Delta^{199}$Hg = 0.01 ± 0.04‰, 1SD), closely resembling dark reduced Hg(0) ($\delta^{202}$Hg = −0.18 ± 0.05‰, $\Delta^{199}$Hg = −0.01 ± 0.03‰, 1SD). In comparison, photoreduced Hg(0) exhibited significant MDF and MIF ($\delta^{202}$Hg = −0.55 ± 0.05‰, $\Delta^{199}$Hg = −0.20 ± 0.07‰, 1SD). In the dark, Hg isotopic signatures remained constant over the temperature range of 15−35 °C. Nonetheless, light exposure and temperature changes together altered Hg(0) MIF signatures significantly. Isotope mixing models along with Hg(0) emission flux data highlighted photo- and microbial reduction contributing 79−88 and 12−21%, respectively, of the total Hg(0) emissions from mining soils, with negligible abiotic dark reduction. Microorganisms are the key driver of soil Hg(0) emissions by first dissolving HgS and then promoting ionic Hg formation, followed by facilitating the photo- and microbial reduction of organically bound Hg. These insights deepen our understanding of the biogeochemical processes that influence Hg(0) releases from surface soils.

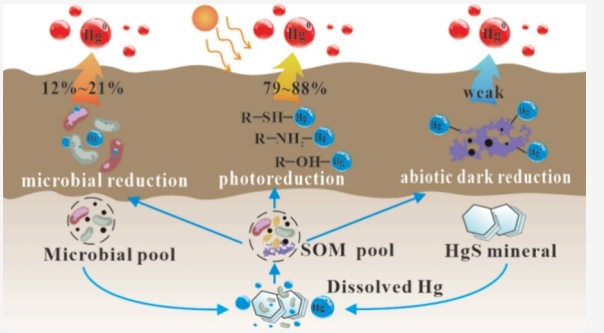


**KEYWORDS:** *soil-atmosphere mercury flux, photoreduction, microbial reduction, HgS dissolution, bioleaching*

## 1. INTRODUCTION

Mercury (Hg), known for its neurotoxic properties, is disseminated globally via atmospheric pathways.[1,2] Elemental mercury (Hg(0)) is the primary form of long distance transport in the atmosphere due to its high stability. Mercury emissions originating from natural sources, including re-emissions of legacy Hg, constitute approximately two-thirds of the total atmospheric Hg inputs.[3] Approximately 80% of the observed data indicates that the exchange of Hg between soil and the atmosphere primarily results in net emissions,[3−5] with annual Hg(0) emissions from soil ranging from 747 to 2900 tons, representing 13 to 36% of global atmospheric Hg emissions.[6,7] The conversion of Hg(II) to Hg(0) is a significant biogeochemical process by which natural Hg is emitted into the atmosphere.[4] Research findings on the pathway of soil Hg(II) reduction identify three primary mechanisms for the production of soil Hg(0): photochemical, microbial, and abiotic dark reduction.[8−10] The photochemical reduction induced by solar radiation is usually recognized as a significant driver of surface soil Hg(0) emissions, as it regulates the diurnal variations in soil-atmosphere Hg(0) exchange flux.[11,12] However, there is still a considerable gap in understanding the effects of microbial reduction and abiotic dark reduction on Hg(0) emissions from soils and their synergistic impacts with photoreduction.

The Wanshan Hg mining area stands out as one of the most affected regions worldwide in terms of surface soil Hg(0) emissions.[13] With original Hg reserves totaling 28,775 tons, Wanshan held the distinction of being the largest in Asia and was dubbed the Mercury Capital of China. Despite the cessation of mining activities in 2001 due to resource exhaustion, the lingering environmental Hg pollution resulting from its extensive history of mining remains unresolved. The persistent and significant Hg(0) emissions from soil have resulted in elevated local air Hg concentrations for an extended period, averaging 111 ± 165 ng m$^{-3}$,[14] which greatly surpasses the global background Hg levels of 1.5 ng m$^{-3}$.[15] Such unusually high soil Hg(0) emissions, via leaf uptake of

Received: May 29, 2024
Revised: September 2, 2024
Accepted: September 3, 2024
Published: September 10, 2024





https://doi.org/10.1021/acs.est.4c05220
*Environ. Sci. Technol.* 2024, 58, 16824−16832

atmospheric Hg, have led to elevated Hg accumulation in rice (27−74 ng $g^{-1}$), a local staple crop, exceeding the Chinese food Hg limit of 20 ng $g^{-1}$.[16] Additionally, human exposure to Hg among local residents is noteworthy, as indicated by hair Hg concentrations ranging from 4 to 53 $\mu g\ g^{-1}$.[17] Accordingly, the Wanshan mine has an extraordinaly Hg environmental transfer pathway, characterized by soil Hg emissions, Hg contamination in atmosphere, and Hg bioaccumulation in crops and local population. A recent study indicated that nighttime soil-atmosphere Hg(0) emission fluxes from farmland, forests, and exposed surfaces in the Wanshan mining area decreased by 78, 37, and 65% respectively compared to daytime levels.[3] Despite the abatement in nighttime soil Hg emission, quantitative data revealed that the emission fluxes remain substantial (94−475 ng $m^{-2}\ h^{-1}$). In line with prior research, solar radiation has been shown to enhance soil Hg(0) emissions in mining regions; however, there remains a dearth of empirical evidence to elucidate the notable nighttime soil Hg(0) emissions. On the other hand, it is puzzling that in the Hg slag landfill, the emission intensity of Hg(0) from surface soil at night (10,147 ng $m^{-2}\ h^{-1}$) is marginally higher than during daytime (9955 ng $m^{-2}\ h^{-1}$).[3] As previously stated, the explanation of these phenomena through photoreduction alone is challenging, suggesting additional factors substantially influencing Hg(0) emissions from surface soil, such as microbial activities. Currently, there is a notable gap in systematic research on soil Hg(0) emissions driven by multiple reduction pathways (i.e., photo-, microbial, and abiotic dark reduction), and in particular, how each pathway contributes to total soil Hg(0) emission under different environmental conditions remains unclear.

To date, reducing soil Hg(0) emissions and air Hg pollution in the Wanshan Mining Area has so far proven to be challenging. The main obstacle is the lack of clarity on the quantitative relevance of the different driving mechanisms of soil Hg(0) emissions, thereby hindering the implementation of effective regulatory measures. Today, stable Hg isotope technology offers a novel approach to improve our understanding of Hg migration and transformation in soils. Mercury is distinguished by its unique three-dimensional isotope tracing system, encompassing mass dependent (MDF), odd mass independent (odd-MIF), and even mass independent fractionation (even-MIF). It is capable of performing quantitative analysis on various Hg biogeochemical processes.[18] In general, most physicochemical processes could result in MDF, whereas only a specific subset of these processes would induce MIF.[18,19] Typically, Hg(0) produced by Hg(II) photoreduction displays significant odd-MIF, with a slope of approximately 1.0 for $\Delta^{199}$Hg versus $\Delta^{201}$Hg.[19] Even-MIF is only observed during the photochemical oxidation/reduction process in the upper atmosphere.[20] While Hg(0) produced by abiotic dark reduction can also exhibit odd-MIF, the magnitude of the fractionation is minimal and the slope of $\Delta^{199}$Hg versus $\Delta^{201}$Hg differs significantly from that of photoreduction.[21] In comparison, the Hg(0) generated through microbial-mediated Hg(II) reduction lacks odd-MIF.[19] As a result, Hg isotope technology can effectively differentiate between various Hg reduction pathways, offering valuable insights for investigating the mechanisms driving soil Hg(0) emissions. In this study, we utilized Hg isotope technology to track the emissions of Hg in the Wanshan surface soil under different reduction mechanisms. The objectives of this study are to quantify the relevance of different driving pathways and associated mechanisms for Hg(0) emissions as well as to provide insights into the biogeochemical cycling of Hg(0) in surface soils.

## 2. MATERIALS AND METHODS

**2.1. Soil Sample Collection and Parameter Testing.** The Wanshan Hg mine is located in the Wanshan District of Tongren City, eastern Guizhou Province, China (27°30′ ∼ 27°32′N, 109°11′ ∼ 109°14′E), which detailed in the Supporting Information (SI), Section S1. (i) Soil sample collection: the top 0−10 cm layer were collected at 11 locations within the Wanshan mining area (Table S1), placed in sterile sampling bags, and transported in a cryogenic storage box with dry ice. (ii) Field experiments: measurements of surface soil-atmosphere Hg(0) flux, soil characteristics, and environmental factors such as soil temperature, moisture content, pH (water/soil = 2.5:1, m/m), and solar radiation intensity were taken at each site. (iii) Laboratory experiments: the soil organic matter (SOM) content was assessed using the potassium dichromate-sulfuric acid titration method, while soil enzyme activities, such as urease, phosphatase, and peroxidase activities, were determined using colorimetric methods, specifically phenol-sodium hypochlorite, disodium phosphate colorimetry, and potassium permanganate titration, respectively. Additional details on these methods can be found in the SI, Section S2.

**2.2. Simulation Experiment of Soil Hg(0) Emissions.** Five experimental configurations were utilized, including the inoculated group (IG), sterilized group (SG), dark group (DG), light group (LG), and SG group with light presence (SG+light). In order to avoid the impact of vegetation on soil-atmospheric Hg flux, experiments were conducted using soil from different plots in bare soil areas. Prior to experiments, the soil sample from the same plot was subjected to various treatments. Specifically, 1.0 kg of fresh soil sieved through a 40 mesh sieve was divided into five groups (IG, SG, DG, LG, SG +light) and placed in glass dishes measuring 30 cm × 30 cm × 15 cm, each with a distinct identifier. The experimental preparations for each group were as follows: (i) IG was treated with 35 mL of Hg-resistant strain WS-B1 suspension, which was isolated from Wanshan soils, cultured in LB liquid medium and 65 mL of sterile deionized water. Additional details on the identification, phylogenetic tree, and Hg removal capabilities of WS-B1 can be found in the SI, Section S3 and Table S6. (ii) The SG and SG+light groups were administered 100 mL of sterile deionized water containing 0.8% Proclin-300, resulting in effective sterilization as detailed in Section S4. (iii) The LG and DG groups were given 100 mL of sterile deionized water. The samples were subjected to gentle agitation at 120 rpm $min^{-1}$ for 20 min in an oscillator to ensure even distribution of bacteria, sterilizing agents, deionized water, and soil. The samples were then placed in a constant temperature incubator set at 37 °C for approximately 15 h to achieve low temperature drying of the soil and remove moisture. Following the restoration of soil moisture to its initial level (200 g), the soils were transferred to 1000 mL borosilicate glass microbial reactors (flux chambers with 10 cm in diameter, 15 cm high, 2 mm wall thickness, and 90% light transmittance). Thereafter, the soil thickness measured approximately 4 cm. The air supply pump, polytetrafluoroethylene filter with a pore size of 0.22 $\mu$m, Tekran zero air filter, and flowmeter were connected in sequence to the air inlet located at the bottom of the reactor. This setup removed airborne particles and Hg from the


https://doi.org/10.1021/acs.est.4c05220
Environ. Sci. Technol. 2024, 58, 16824−16832

incoming air, allowing for the collection of emitted Hg(0) from the soil (Figure S1). The ventilation flow rate was set at 400 mL $min^{-1}$. The air carrying soil-emitted Hg exited through the top outlet of the reactor, passed through a polytetrafluoroethylene filter again to prevent soil particle resuspension, and was directed toward a 5.0 mL reverse aqua regia solution ($HNO_3$/HCl = 2:1, v/v) to capture emitted Hg from the soil. The Hg isotope compositions in the trapping solutions reflected the Hg isotope fractionation of Hg(0) emitted from the soils.

These experimental trials were carried out at 15 and 35 °C within a constant temperature incubator. To control for light exposure, the experimental groups LG and SG+light utilized an LED solar analog lamp (300−800 nm) positioned 5 cm above the flux chamber, with a measured light intensity of 72 $\mu$w $cm^{-2}$ inside the flux chamber. The side walls of the flux chambers were covered with tin foil, allowing only the surface soil to be exposed to light, while all other experimental groups were conducted in darkness. The mean system Hg blank of a 5.0 mL reverse aqua regia trap during 24 h of operation was found to be 0.19 ng $mL^{-1}$ at 15 °C and 0.74 ng $mL^{-1}$ at 35 °C, representing a negligible contribution (<6%) compared to the Hg content collected from each treatment (Table S2). Furthermore, the utilization of reverse aqua regia for the collection of Hg(0) has been extensively employed in previous research on Hg isotopes, with validated high Hg recovery rates and results that do not introduce significant bias in Hg isotope compositions.[3,22,23]

**2.3. Microbial HgS Dissolution.** *Shewanella oneidensis* MR-1 is a significant model electrogenic bacterium and a prevalent Gram-negative facultative anaerobe in sedimentary environments. The status of it as a representative dissimilatory iron-reducing bacterium (DIRB) has been extensively acknowledged, prompting substantial research endeavors centered on this microorganism.[24−26] Here, *Shewanella oneidensis* MR-1 (Beijing Biobw Biotechnology Co., Ltd.) was applied to investigate its potential to dissolve HgS. A 5.0 mL aliquot of activated cultured MR-1, 0.4 g of humic acid, and 0.1 g of HgS (Aladdin Biochemical Technology Co., Ltd.) were added to 45 mL of LB liquid culture medium. The control experiment was conducted on sterile cell suspension concurrently. Triplicate experiments were carried out to assess reproducibility. The suspension was filtered using 0.22 $\mu$m membrane syringe filters (13 mm diameter) to eliminate bacterial cells and solid HgS, followed by analysis of the Hg content in the suspension. The sorption of Hg on the membrane filters was assessed using LB medium containing a 300 ng $mL^{-1}$ $HgCl_2$ solution, with a recovery rate of 95−98% ($n$ = 5).

**2.4. Hg Content, Soil Hg(0) Emission Flux, and Hg Isotope Measurements.** *2.4.1. Hg Content Measurements.* The Hg(0) concentrations in air were measured using the RA-915 Hg analyzer (Lumex Ltd.). Continuous monitoring was done at a height of 1.0 m above the surface for 3 min, with average values recorded (SI, Section S5). Soil Hg concentrations were measured with the DMA-80 Hg analyzer, with the average value of three repeated measurements per sample reported. Hg contents in the trapping solutions were determined using cold vapor atomic fluorescence spectrometry (CVAFS, Model 2500, Tekran Instruments).

*2.4.2. Soil Hg(0) Emission Flux.* The Aerodynamic Flux Chamber (DFC) technique was utilized, as described in previous literature,[27] to determine the Hg(0) emission flux at the soil-atmosphere interface in field. The Hg(0) emission fluxes ($F_{Hg}$, ng $m^{-2}$ $h^{-1}$) were calculated by the eq 1. In laboratory simulations, Hg(0) emissions from soil were captured with reverse aqua regia solution to calculate the soil Hg(0) emission fluxes. The $F_{Hg}$ values in simulation experiments were calculated based on eq 2.[28]

$$F_{Hg} = Q(C_{out} - C_{in})/A_0 \quad (1)$$

$$F_{Hg} = M_{Hg}/(H \times A_1) \quad (2)$$

where, $C_{out}$ and $C_{in}$ represent Hg(0) concentrations (ng $m^{-3}$) in the DFC outlet and ambient air, respectively. $Q$ is the flow rate through the DFC. The shear stresses in DFC are uniform and the sidewall effect is minimal at a gas flow rate of 15 L $min^{-1}$.[27] Therefore, $Q$ is set to 15 L $min^{-1}$ in this study. $A_0$ represents the effective surface area of the soil covered by the DFC, which is 0.09 $m^2$. $M_{Hg}$ represents the Hg mass emitted from soil collected in the aqua regia (ng). $A_1$ represents the cross-sectional area of the flux chamber, measured at 78.5 $cm^2$. $H$ represents the duration of Hg collection (h).

*2.4.3. Hg Isotope Compositions.* The Neptune Plus MC-ICP-MS used for Hg isotopic analyses employed an online Hg(0) vapor generation system for sample introduction and a desolvating nebulizer for Tl internal standard (NIST SRM 997) introduction. The measurements were calibrated using standard-bracketing with NIST3133, following our previously published methods.[22,23] The results of the MDF and MIF analyses were reported as[29]

$$\delta^{202}Hg(‰) = [(^{202}Hg/^{198}Hg)sample/(^{202}Hg/^{198}Hg)_{NIST3133} - 1] \times 1000 \quad (3)$$

$$\Delta^{199}Hg(‰) = \delta^{199}Hg - (0.252 \times \delta^{202}Hg) \quad (4)$$

$$\Delta^{200}Hg(‰) = \delta^{200}Hg - (0.502 \times \delta^{202}Hg) \quad (5)$$

$$\Delta^{201}Hg(‰) = \delta^{201}Hg - (0.752 \times \delta^{202}Hg) \quad (6)$$

A standard reference NIST 3177 was analyzed repeatedly to obtain the analytical uncertainty of isotopic compositions during instrumental procedures. The isotopic compositions of NIST 3177 ($\delta^{202}$Hg = −0.51 ± 0.10‰, $\Delta^{199}$Hg = −0.01 ± 0.06‰, $\Delta^{200}$Hg = 0.00 ± 0.05‰, and $\Delta^{201}$Hg = −0.01 ± 0.08‰, 2 SD, $n$ = 20), agreed with previously reported values.[30,31] In addition, isotopic compositions of standard references of GSS-4 ($\delta^{202}$Hg = −1.60 ± 0.09, $\Delta^{199}$Hg = −0.45 ± 0.06, $\Delta^{200}$Hg = 0.00 ± 0.07, and $\Delta^{201}$Hg = −0.41 ± 0.07‰, 2 SD, $n$ = 5) were also measured and consistent with previously published results.[32]

**2.5. Hg Isotope Mixing Model.** Soil Hg(0) emissions result from the photoreduction of Hg(II) on the soil surface, as well as microbial and abiotic dark reduction in deeper soil layers.[22] In the case of Wanshan soil, microbial reduction was found to be the major driver of Hg(0) emission under dark conditions, with abiotic dark reduction playing a minimal role (as discussed in Section 3.2). Thus, the isotope mixing model (eqs 7 and 8) was employed to estimate the relative contributions of photoreduction and dark reduction (encompassing both microbial and abiotic processes) to soil Hg(0) emissions.

$$\Delta^{199}Hg_{LG} = F_{pho} * \Delta^{199}Hg_{pho} + F_{DG} * \Delta^{199}Hg_{DG} \quad (7)$$

$$F_{pho} + F_{DG} = 1 \quad (8)$$



https://doi.org/10.1021/acs.est.4c05220
Environ. Sci. Technol. 2024, 58, 16824−16832

where, $\Delta^{199}Hg_{LG}$, $\Delta^{199}Hg_{pho}$, and $\Delta^{199}Hg_{DG}$ represent the $\Delta^{199}Hg$ signatures of Hg(0) in the total soil emission product under light exposure (affected by microbial reduction, abiotic dark reduction, and photoreduction), soil emission product solely influenced by photoreduction, and soil emission product under dark conditions, respectively (unit: ‰). $F_{pho}$ and $F_{DG}$ represent the proportionate contributions of Hg(0) emitted through photoreduction and dark reduction, respectively (unit: %).

## 3. RESULTS AND DISCUSSION

**3.1. Air Hg Concentration and Soil-Atmosphere Hg(0) Exchage Flux in the Field.** Air Hg(0) concentrations in the Wanshan mining area (15−185 ng $m^{-3}$, $n$ = 55, Table S1) were significantly higher than global (1.5 ng $m^{-3}$)[15] and local (2.3−4.4 ng $m^{-3}$)[14] background levels. The majority of soil-atmosphere Hg(0) exchange measurements yielded positive values (200−5670 ng $m^{-2}$ $h^{-1}$, $n$ = 10), indicating that soil serves as a net emission source of Hg(0). The sole instance of a negative value was identified in the surface soil of a residential area (−70 ng $m^{-2}$ $h^{-1}$), potentially attributed to human activities leading to soil compaction and reduced solar radiation during monitoring. Analogous to the emissions observed in the Wanshan mining region, substantial surface soil Hg(0) emissions have been documented at other Hg mining sites, such as the Idrija Hg mining area in Slovenia (71−702 ng $m^{-2}$ $h^{-1}$)[33] and the El Callao Hg-gold amalgamation mining area in Venezuela (9−239 $\mu$g $m^{-2}$ $h^{-1}$).[34] The flux of Hg(0) emissions from surface soils at Hg mining sites is significantly higher, by three to 5 orders of magnitude, compared to the global background soil-atmosphere Hg(0) flux (1−69 ng $m^{-2}$ $h^{-1}$).[33−36]

**3.2. Hg(0) Emissions from Soils in Laboratory Simulations.** Figure 1 illustrates the Hg(0) emission fluxes from the soils of various treatments (DG, SG, IG, LG, and SG +light soils) at two distinct temperatures. SG and IG were selected as representatives to elucidate the impact of abiotic dark reduction and microbial reduction on soil Hg(0) emissions, with DG serving as a comprehensive representation of these processes in natural soil in the dark. While IG may include some influences from abiotic dark reduction, its contribution is deemed negligible in comparison with microbial reduction (as discussed below), and is therefore inconsequential for the purposes of this study.

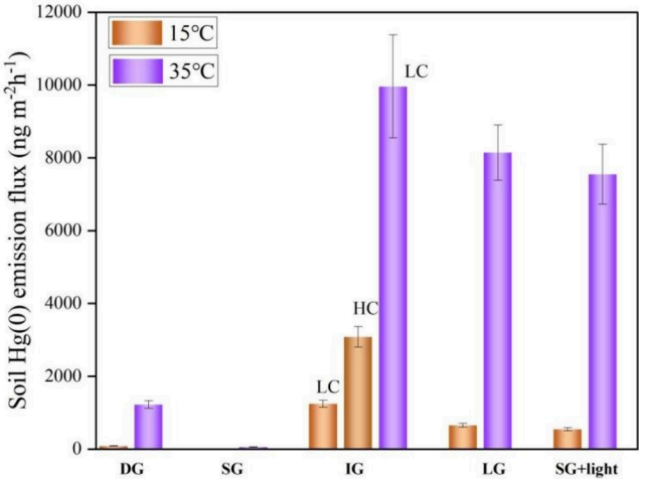


**Figure 1.** Soil Hg(0) emission fluxes of dark groups (DG), sterilized group (SG), inoculated group (IG), light group (LG), and SG group with light presence (SG+light) under 15 and 35 °C. Error bars represent 1 SD of the parallel experiments. LC: low-dose inoculation group; HC: high-dose inoculation group.

At 15 °C, the Hg(0) emission fluxes for DG and SG were measured to be 86 ± 10 ng $m^{-2}$ $h^{-1}$ (1SD, $n$ = 4) and 7 ± 1 ng $m^{-2}$ $h^{-1}$ (1SD, $n$ = 4), respectively. The calculated Hg(0) emission flux of SG was found to be only 8% of DG, with the quantitative data of Hg content in the trap solution approaching the system blank (Table S2). These findings suggest the minimal contribution of abiotic dark reduction to soil Hg(0) emissions, while microbial reduction plays a dominant role in the absence of light, as evidenced from IG. Adding a low-dose bacterial solution (IG-LC), there was a notable increase in Hg(0) emission flux, reaching 1246 ± 97 ng $m^{-2}$ $h^{-1}$ (1SD, $n$ = 3). Furthermore, Hg(0) emission fluxes were observed to increase with the quantity of bacteria added. A comparison between IG-LC and IG-HC revealed a 2.3-fold increase in bacterial content ($2.1 \times 10^7$ vs $4.9 \times 10^7$ cell $g^{-1}$ soil) and a corresponding 2.5-fold increase in Hg(0) emission flux (1246 ± 97 vs 3082 ± 283 ng $m^{-2}$ $h^{-1}$, 1SD). Such findings underscore the significant role and potential impact of microorganisms in facilitating soil Hg(0) emissions. The process by which biotic reduction of Hg(II) is achieved is intricately linked to the mer operon of microorganisms, primarily regulated by the MerA and MerB genes.[37,38] The observed increase in Hg(0) emission fluxes from DG and IG soils by 14.3 and 8.0 times, respectively, with a temperature jump from 15 to 35 °C. Such promoting effect of temperature rise on Hg(0) emissions consistent with field studies.,[39,40] which may be due to increased microbial activity resulting in elevated levels of volatile Hg and vapor pressure. With increasing temperature, microbial activity is consistently the primary driver of Hg(0) emissions in dark reduction, as opposed to the minimal contribution of abiotic reduction (<2%, Table S2).

SG+light experiments revealed that Hg(0) emission fluxes under lighting conditions at 15 °C (543 ± 43 ng $m^{-2}$ $h^{-1}$, 1SD, $n$ = 4) and 35 °C (7547 ± 825 ng $m^{-2}$ $h^{-1}$, 1SD, $n$ = 4) were 5.3 and 6.2 times higher than those of the DG group at corresponding temperatures. Furthermore, the combined Hg(0) emission fluxes of SG+light and DG were comparable to the Hg(0) flux of LG (Table S2), suggesting a synergistic effect and equilibrium relationship among different Hg reduction pathways. Under simulated experimental conditions, the relative contributions of photoreduction, microbial reduction, and abiotic dark reduction to soil Hg(0) emissions were determined to be 84, 15, and 1% at 15 °C, and 86, 13, and 1% at 35 °C, respectively. This indicates that in the surface bare soil at Hg mining sites, Hg(0) emissions are primarily controlled by photoreduction, followed by microbial reduction, with negligible contribution from abiotic dark reduction.

**3.3. Isotopic Composition of Hg(0) Emitted via Different Reduction Pathways.** Figures 2 and S2 display the isotopic compositions of Hg(0) emitted from IG, DG, LG, and SG+light soils. Since SG soil-emitted Hg(0) was close to the system blank, quantifying its isotopic composition was impossible (Table S2). At 15 °C (Figure 2a), The Hg(0) emitted from IG soil exhibited negative $\delta^{202}Hg$ values of −0.30 ± 0.08‰ (1SD, $n$ = 6) and near-zero $\Delta^{199}Hg$ values of 0.01 ± 0.04‰ (1SD, $n$ = 6). These results supports the argument that microbial Hg reduction does not lead to significant odd-MIF.[18]


https://doi.org/10.1021/acs.est.4c05220
Environ. Sci. Technol. 2024, 58, 16824−16832

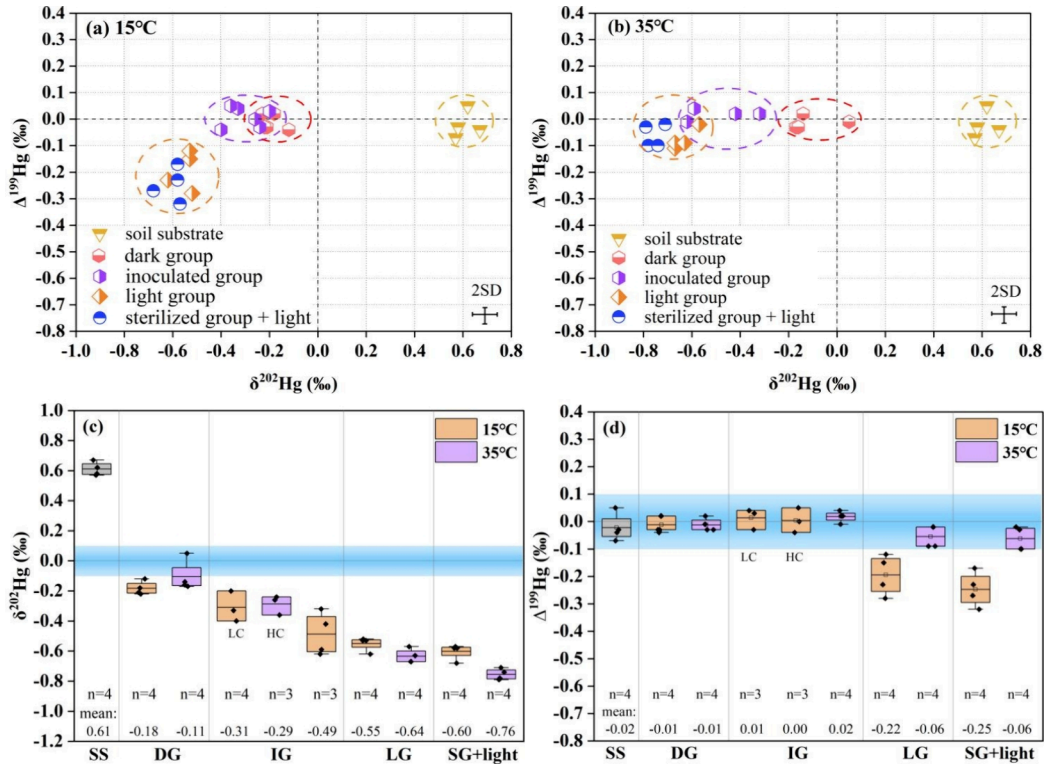


**Figure 2.** $\Delta^{199}$Hg versus $\Delta^{201}$Hg plot of soil substrate (SS) and Hg(0) emitted from the soils of dark groups (DG), inoculated groups (IG), light groups (LG), and sterilized groups with light presence (SG+light) at 15 and 35 °C. The bacterial addition concentrations for the low-dose inoculation group (IG-LC) and high-dose inoculation group (IG-HC) were $4.9 \times 10^7$ cell $g^{-1}$ soil (8% of 1SD, $n = 3$) and $2.1 \times 10^7$ cell $g^{-1}$ soil (11% of 1SD, $n = 3$), respectively. Error bars are 2SD analytical uncertainty of $\Delta^{199}$Hg and $\Delta^{201}$Hg. The slope of $\Delta^{199}$Hg versus $\Delta^{201}$Hg of various experimental groups shown in Figure S4.

Wherein, the $\delta^{202}$Hg values for IG-LC and IG-HC were determined to be −0.31 ± 0.10‰ (1SD, $n = 3$) and −0.29 ± 0.06‰ (1SD, $n = 3$), respectively, while the $\Delta^{199}$Hg values were 0.01 ± 0.04‰ (1SD, $n = 3$) and 0.00 ± 0.05‰ (1SD, $n = 3$). There were no statistically significant differences in $\Delta^{199}$Hg or $\delta^{202}$Hg ($t$ test, both $p > 0.05$) between IG-LC and IG-HC, indicating that The small variations in the amount of bacteria added had no significant effect on the isotopic composition of Hg(0) released by microbial reduction. The isotopic compositions of Hg(0) emitted from DG soil were comparable to those from IG soil, exhibiting negative $\delta^{202}$Hg (−0.18 ± 0.05‰, 1SD, $n = 4$) and near-zero $\Delta^{199}$Hg (−0.01 ± 0.03‰, 1SD, $n = 4$). The $\Delta^{199}$Hg versus $\Delta^{201}$Hg plot in Figure 2a,b demonstrates a close relationship in the isotope compositions of Hg(0) emitted from, suggesting the potentially significant contribution of microbial-driven soil Hg(0) emission in the absence of light, as reflected by the results of soil Hg(0) emission flux discussed in Section 3.2. LG-emitted Hg(0) had the most negative $\delta^{202}$Hg (−0.55 ± 0.05‰, 1SD, $n = 4$) and negative $\Delta^{199}$Hg (−0.20 ± 0.07‰, 1SD, $n = 4$) compared to the others, mirroring MIF due to lighter isotope escape under light-driven conditions.[18,41]

At 15 and 35 °C, the $\delta^{202}$Hg values of various soil emitted Hg(0) displayed a consistent pattern of LG < IG < SS (Figure 2c,d), suggesting the preferential reduction of lighter Hg isotopes of by light, followed by microbial processes. In comparison, heavier Hg isotopes remain in the soil. With increasing temperature, Hg(0) emitted from LG and IG generated negative $\delta^{202}$Hg shifts with mean values of −0.19 and −0.09, respectively This indicates that elevated temperature may exacerbate the preference for Hg isotopic in photoreduction and microbial reduction.

The $\Delta^{199}$Hg values of various soil emitted Hg(0) were in the order of LG < IG ≈ SS. Increasing the temperature from 15 to 35 °C, the $\Delta^{199}$Hg shift of IG emitted Hg(0) was insignificant ($t$ test, $p > 0.05$), whereas LG-emitter Hg(0) cause a significantly positive shift of 0.16 ($t$ test, $p < 0.01$). Field monitoring data revealed an increase in MIF of soil-emitted Hg(0) with increasing solar radiation.[3] Nevertheless, our Hg isotope data suggests that under light conditions, elevated temperatures also result in a positive MIF shift during Hg(II) reduction to Hg(0). Previous studies have indicated that net MIF during Hg(II) reduction is the result of (+)MIF and (−)MIF co-occurrence. Specifically, Hg(II) bound to S and N ligands shows (+) MIF during the photoreaction, while Hg(II) bound to O ligands has (−)MIF.[21,42−44] Meanwhile, differences in the photoreduction rates of various ligands binding to Hg(II) have also been observed. Low-molecular-weight organic compounds containing reduced S ligands, e.g., cysteine and glutathione, exhibit slower Hg(II) photochemical reduction compared to those lacking reduced S ligands, e.g., serine and oxalic acid.[42] It is postulated that temperature may impact the photoreduction rate of different ligands binding to Hg(II). Consequently, the phenomenon can be explained as the O-ligand bound Hg(II) with a higher photoreduction rate contributing to the (−)MIF development at low temperatures under the light. As temperatures increase, the photoreduction rate of the S and N ligand-binding-Hg(II) increases, resulting in a partial offset of (−)MIF and (+)MIF, as well as an overall MIF increase.


https://doi.org/10.1021/acs.est.4c05220
Environ. Sci. Technol. 2024, 58, 16824−16832

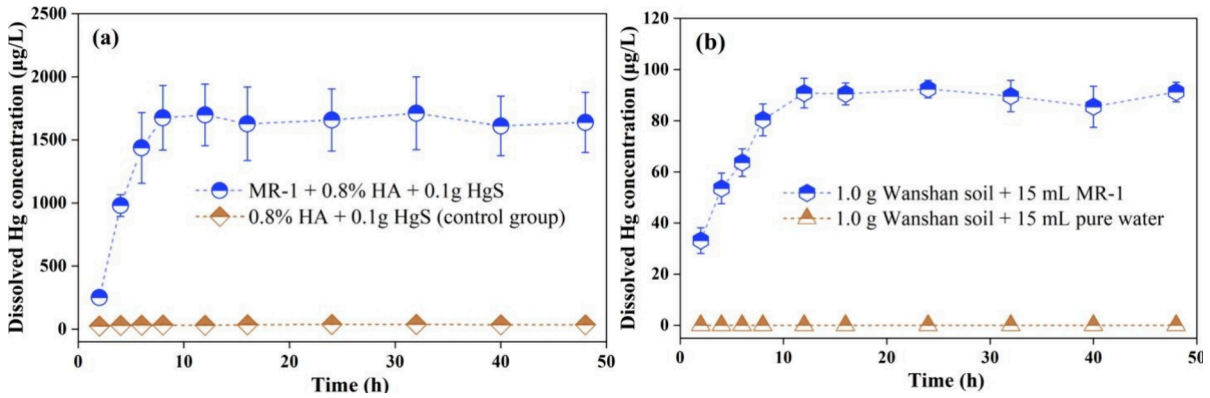


**Figure 3.** Dissolved Hg concentration variation in the suspension during HgS bioleaching process by *Shewanella oneidensis* MR-1. The bacterial concentrations of MR-1 added was $1.5 \times 10^7$ cell $mL^{-1}$ (13% of 1SD, $n = 3$). The Hg content and SOM content of the Wanshan soil used for biological dissolution validation are 11.33 mg $kg^{-1}$ and 57.12 g $kg^{-1}$, respectively. Error bars represent 1SD of three parallel experiments.

**3.4. Contributions of Different Hg Reduction Pathways.** Since abiotic dark reduction contributes generally trace to total soil Hg(0) emissions (see Section 3.2), we are able to assume that the SG soil Hg(0) emissions from SG soils are predominately driven by microbial reduction, while the emissions from SG+light soils are mainly driven by photoreduction. Considering SG+light and DG soil emitted Hg(0) as the end-members of light reduction and nonlight reduction, the relative contributions of photoreduction and microbial reduction to soil Hg(0) emissions can be quantified (formulas 7 and 8). Based on the binary mixing model output with $\Delta^{199}$Hg as an inert tracer, photoreduction accounted for 79 ± 15% (1SD, $n = 4$) of total Hg(0) emissions at 15 °C, with microbial reduction contributing 21 ± 15% (1SD, $n = 4$). At 35 °C, the contributions of Hg(0) emissions via photo- and microbial reduction were 88 ± 10 and 12 ± 10% (1SD, $n = 4$), respectively. Accordingly, the relative contribution of photoreduction to Hg(0) emissions from soils appears to increase with increasing temperature.

Additionally, the contribution of soil Hg(0) emissions between photoreduction and microbial reduction, as determined by the Hg isotope mixing model, coincides with the Hg(0) emission flux results (Table S3). The combination of these two methods effectively confirms the relative impact of different pathways for soil Hg(0) emissions.

**3.5. Correlations between Organic Matter, Enzyme Activity, and Hg in Soil.** Mercury contents in the surface soil ranged from 3.16 to 21.12 mg $kg^{-1}$, with an average of 12.04 mg $kg^{-1}$ ($n = 11$, Table S1) and correlated strongly with organic matter levels in soils (Figure S3a–d). Mercury ions possess a high electron affinity and are capable of forming covalent bonds with organic functional groups that contain electron donors such as S, O, and N, including thiol (−SH), carbonyl (−C=O), carboxyl (−COOH), hydroxyl (−OH), and amino ($-NH_2$) groups.[45−47] Enzymes within soil organic matter (SOM) are a group of proteins with biocatalytic properties, primarily originating from microorganisms, root exudates, and the decomposition of animal and plant residues.[48,49] Also, Hg contents correlated with different soil enzyme activities, particularly the notably negative correlation with urease activity ($R^2 = 0.79$, $p < 0.01$), over peroxidase activity ($R^2 = 0.46$, $p < 0.01$) and phosphatase activity ($R^2 = 0.45$, $p < 0.01$) (Figure S3b–d). This negative correlation can be considered from two perspectives: the toxic inhibitory effect of Hg on microbial activity and microbial-driven Hg migration. For instance, Hg can form stable chemical bonds with sulfhydryl (−SH) and imidazole ligands ($Hg^{2+} + 2C_3H_4N_2 \rightleftharpoons Hg(C_3H_4N_2)_2^{2+}$) in the active sites of soil enzymes, leading to noncompetitive inhibition with substrates and partial deactivation of soil enzymes.[50,51] Additionally, some Hg-resistant bacteria possess genes encoding for Hg reductase (merA) and organic Hg lyase (merB), which contribute to Hg emissions from soils.[52,53] Liang et al. suggested that microbial growth plays a important role in the accumulation of SOM by depositing microbially derived carbon into the SOM reservoir through biomass turnover and necrotic mass accumulation.[54] This is supported by a positive correlation between soil enzyme (urease) activity and SOM content ($R^2 = 0.53$, $p < 0.01$, Figure S3e), indicating the potential contribution of microorganisms to the SOM reservoir. This relationship implies that microorganisms may collectively regulate both Hg content and organic matter level in soil.

**3.6. Microbial Dissolution of HgS.** Extended X-ray absorption fine structure spectroscopy and sequential extraction evidenced the predominance of HgS in Wanshan soils (>80% of total Hg).[55−57] Given its insolubility, HgS has long been considered to be biologically inert and a minor participant in Hg biogeochemical cycling.[58] Surprisingly, although the water-soluble fraction represented <0.5% of total Hg in Wanshan soils, the corresponding pool (0.05 to 0.49 μg $g^{-1}$, $n = 8$)[47] was still remarkable, for which plausible explanations are still lacking. Recently, the bioavailability of HgS has been revealed by microbial transformation of HgS to MeHg e.g., sulfate-reducing bacteria,[58,59] delivering potential insights into the cause of high water-soluble Hg concentrations in soils from mining areas.

Figure 3a shows the rapid increase of dissolved Hg concentrations from 251.0 to 1676.2 μg $L^{-1}$ within the first 8 incubation hours in the HgS-humic acid-microbe (*S. pneidensis* MR-1) ternary system, reflecting distinctly HgS dissolution due to the presence of MR-1. Conversely, he release of dissolved Hg in the control was constantly and comparably trace (<40 μg/L) throughout the incubation. It can therefore be inferred that certain soil microorganisms capable of dissolving HgS, e.g., via proton sorption to mineral surfaces by microorganisms and electron transfer,[60] promoting the breaking of Hg−S bond. Such hypothesis was also confirmed by the similar bioleaching effect of MR-1 on Wanshan soils (Figure 3b).


https://doi.org/10.1021/acs.est.4c05220
Environ. Sci. Technol. 2024, 58, 16824−16832

Thus, the high Hg(0) emissions from the Hg slag landfills in Zhu et al. (2022)[3] are most likely the result of microbially promoted Hg dissolution. Moreover, organic matter (OM) could complex HgS which facilitates microbial enrichment, thereby inhibiting HgS precipitation and promoting HgS dissolution.[61,62] With microbial involvement, SOM plays a key role in Hg dissolution and subsequent photoreduction and microbial reduction of Hg(II) to Hg(0), affecting gaseous losses and biotransformation of Hg.

Here, we propose that Hg(0) emissions from soils in the Wanshan mining area occurred via (1) microbial HgS dissolution facilitated by OM-Hg complex formation and then followed by (2) Hg(II) reduction to Hg(0), mainly via photo- and microbial reduction. In particular, certain Hg complexes (e.g., mercuric thiols) are more mobile and available for organisms.[56,63] In the presence of microorganisms with Hg metabolism function, Hg(II) is reduced to Hg(0) and sunsequently emitted from soils.[37,38] Today, the mechanism of Hg(II) photoreduction is still unclear, although direct and indirect photolysis theories have been proposed.[21,64,65] The former explanation is based on the absorption of photons by Hg complexes leading to the homologous cleavage of Hg ligand bonds, while the latter explanation is related to the reaction between Hg complexes and photochemical reactants. Although the contribution of microbial directly driven Hg(0) emissions is relatively small, microbial HgS dissolution may provide a leading condition for the formation of soil organic Hg and play an indirect role in Hg(0) emissions under photoreduction. Abiotic dark reduction to soil Hg(0) emissions are so low that it is nigiligible.

## 4. IMPLICATIONS

The output of the binary Hg isotope mixing model is consistent with the soil Hg(0) emission flux, suggesting photo- and microbial reduction as the primary mechanisms driving surface soil Hg(0) emissions in the Wanshan mining area, explaining approximately 79−88 and 12−21% of total Hg(0) emissions, respectively. In comparison, the contribution of abiotic dark reduction is extremely low. Two important processes affecting the fate of soil Hg(0) emissions were inferred. Although the contribution of microbial reduction is minor, microbe-mediated HgS dissolution could increase the dissolved Hg pool to complex with organic ligands in soils, providing advantageous conditions for photo- and microbial reduction. Therefore, from a long-term perspective, antibacterial strategies may be a feasible to control soil Hg(0) emissions and air Hg pollution in Wanshan mining area, and needs to be further validated in future research. Our results not only provide explanatory evidence for the persistently high surface Hg(0) fluxes observed in Hg mining areas worldwide but also deliver insights into the microbial involvement in global soil Hg emissions and Hg cycling.

## ASSOCIATED CONTENT

### Supporting Information

The Supporting Information is available free of charge at https://pubs.acs.org/doi/10.1021/acs.est.4c05220.

Site description of the research area, determination of soil enzyme activity, isolation, identification, and neighbor-joining phylogenetic tree of strain WS-B1, soil sterilization operation, measurement of Hg(0) concentration, concentration analysis of inoculated bacteria, correlation between Hg content, organic matter content, and enzyme activity in the soil, collection and Hg isotopic composition of Hg(0) emitted from the soil, and the data sets pertaining to soil-atmospheric Hg(0) flux and associated environmental factors (PDF)

## AUTHOR INFORMATION


### Corresponding Author

**Xinbin Feng** − *State Key Laboratory of Environmental Geochemistry, Institute of Geochemistry, Chinese Academy of Sciences, Guiyang 550081, China; University of Chinese Academy of Sciences, Beijing 100049, China;* orcid.org/0000-0002-7462-8998; Email: fengxinbin@vip.gyig.ac.cn

### Authors

**Qingyi Cao** − *State Key Laboratory of Environmental Geochemistry, Institute of Geochemistry, Chinese Academy of Sciences, Guiyang 550081, China; Key Laboratory of Karst Georesources and Environment (Guizhou University), Ministry of Education, Guiyang 550025, China*

**Haiyan Hu** − *State Key Laboratory of Environmental Geochemistry, Institute of Geochemistry, Chinese Academy of Sciences, Guiyang 550081, China;* orcid.org/0000-0002-5768-6731

**Wei Yuan** − *State Key Laboratory of Environmental Geochemistry, Institute of Geochemistry, Chinese Academy of Sciences, Guiyang 550081, China;* orcid.org/0000-0003-3329-2081

**Jen-How Huang** − *State Key Laboratory of Environmental Geochemistry, Institute of Geochemistry, Chinese Academy of Sciences, Guiyang 550081, China; Environmental Geosciences, University of Basel, Basel 4056, Switzerland*

**Xuewu Fu** − *State Key Laboratory of Environmental Geochemistry, Institute of Geochemistry, Chinese Academy of Sciences, Guiyang 550081, China;* orcid.org/0000-0002-5174-7150

Complete contact information is available at: https://pubs.acs.org/10.1021/acs.est.4c05220


### Notes

The authors declare no competing financial interest.

## ACKNOWLEDGMENTS

This work was supported by the National Natural Science Foundation of China (No. 42407351 and 42394090), Guizhou Provincial 2019 Science and Technology Subsidies (No. GZ2019SIG), and Foundation of State Key Laboratory of Karst Georesources and Environment (Guizhou University) (No. KST202406). We extend our gratitude to Dr. Chen Jinquan of Yunnan University for providing assistance in the isolation of soil bacteria.

## REFERENCES

(1) Mason, R. P.; Choi, A. L.; Fitzgerald, W. F.; Hammerschmidt, C. R.; Lamborg, C. H.; Soerensen, A. L.; Sunderland, E. M. Mercury biogeochemical cycling in the ocean and policy implications. *Environ. Res.* **2012**, *119*, 101−117.

(2) Sonke, J. E.; Angot, H.; Zhang, Y.; Poulain, A.; Björn, E.; Schartup, A. Global change effects on biogeochemical mercury cycling. *Ambio* **2023**, *52*, 853−876.

(3) Zhu, W.; Fu, X.; Zhang, H.; Liu, C.; Skyllberg, U.; Sommar, J.; Yu, B.; Feng, X. Mercury Isotope Fractionation during the Exchange of Hg(0) between the Atmosphere and Land Surfaces: Implications

for Hg(0) Exchange Processes and Controls. *Environ. Sci. Technol.* **2022**, *56*, 1445−1457.
(4) Obrist, D.; Pokharel, A. K.; Moore, C. Vertical profile measurements of soil air suggest immobilization of gaseous elemental mercury in mineral soil. *Environ. Sci. Technol.* **2014**, *48*, 2242−2252.
(5) Agnan, Y.; Le Dantec, T.; Moore, C. W.; Edwards, G. C.; Obrist, D. New Constraints on Terrestrial Surface Atmosphere Fluxes of Gaseous Elemental Mercury Using a Global Database. *Environ. Sci. Technol.* **2016**, *50*, 507−524.
(6) Smith-Downey, N. V.; Sunderland, E. M.; Jacob, D. J. Anthropogenic impacts on global storage and emissions of mercury from terrestrial soils: Insights from a new global model. *J. Geophys. Res.: Biogeosci.* **2010**, *115*, G03008.
(7) Amos, H. M.; Jacob, D. J.; Streets, D. G.; Sunderland, E. M. Legacy impacts of all-time anthropogenic emissions on the global mercury cycle. *Global Biogeochem. Cycles* **2013**, *27*, 410−421.
(8) Xin, M.; Gustin, M. S. Gaseous elemental mercury exchange with low mercury containing soils: investigation of controlling factors. *Appl. Geochem.* **2007**, *22* (7), 1451−1466.
(9) Fritsche, J.; Obrist, D.; Alewell, C. Evidence of microbial control of Hg(0) emissions from uncontaminated terrestrial soils. *J. Plant Nutr. Soil Sci.* **2008**, *171*, 200−209.
(10) Jiang, T.; Skyllberg, U.; Wei, S. Q.; Wang, D. Y.; Lu, S.; Jiang, Z. M.; Flanagan, D. C. Modeling of the structure-specific kinetics of abiotic, dark reduction of Hg(II) complexed by O/N and S functional groups in humic acids while accounting for time-dependent structural rearrangement. *Geochim. Cosmochim. Acta* **2015**, *154*, 151−167.
(11) Gao, Y.; Wang, Z.; Zhang, X.; Wang, C. Observation and estimation of mercury exchange fluxes from soil under different crop cultivars and planting densities in North China Plain. *Environ. Pollut.* **2020**, *259*, No. 113833.
(12) Choi, H. D.; Holsen, T. M. Gaseous mercury emissions from unsterilized and sterilized soils: The effect of temperature and UV radiation. *Environ. Pollut.* **2009**, *157* (5), 1673−1678.
(13) Peng, H.; Rong, Y.; Chen, D.; Sun, R.; Huang, J.; Ding, H.; Olid, C.; Yan, H. Anthropogenic activity and millennial climate variability affect Holocene mercury deposition of an alpine wetland near the largest mercury mine in China. *Chemosphere* **2023**, *316*, No. 137855.
(14) Du, B.; Yin, R.; Fu, X.; Li, P.; Feng, X.; Maurice, L. Use of mercury isotopes to quantify sources of human inorganic mercury exposure and metabolic processes in the human body. *Environ. Int.* **2021**, *147*, No. 106336.
(15) Jaffe, D.; Prestbo, E.; Swartzendruber, P.; Weiss-Penzias, P.; Kato, S.; Takami, A.; Hatakeyama, S.; Kajii, Y. Export of atmospheric mercury from Asia. *Atmos. Environ.* **2005**, *39* (17), 3029−3038.
(16) Pei, P.; Mu, D.; Ma, W.; Sun, T.; Sun, Y. Characteristic of Mercury and Methylmercury Pollution in Paddy Soils around Mercury Mine Area and Its Ecological Risk. *J. Ecol. Rural Environ.* **2022**, *38* (1), 112−119.
(17) Xing, X.; Du, R.; Li, Y.; Li, B.; Cai, Q.; Mo, G.; Gong, Y.; Chen, Z.; Wu, Z. Structural change of human hair induced by mercury exposure. *Environ. Sci. Technol.* **2013**, *47* (19), 11214−11220.
(18) Blum, J. D.; Sherman, L. S.; Johnson, M. W. Mercury isotopes in earth and environmental sciences. *Annu. Rev. Earth Planet. Sci.* **2014**, *42*, 249−269.
(19) Blum, J. D.; Bergquist, B. A. Reporting of variations in the natural isotopic composition of mercury. *Anal. Bioanal. Chem.* **2007**, *388*, 353−359.
(20) Chen, J. B.; Hintelmann, H.; Feng, X. B.; Dimock, B. Unusual fractionation of both odd and even mercury isotopes in precipitation from Peterborough, ON Canada. *Geochim. Cosmochim. Acta* **2012**, *90*, 33−46.
(21) Zheng, W.; Hintelmann, H. Nuclear Field Shift Effect in Isotope Fractionation of Mercury during Abiotic Reduction in the Absence of Light. *J. Phys. Chem. A* **2010**, *114* (12), 4238−4245.
(22) Chen, C. Y.; Huang, J. H.; Li, K.; Osterwalder, S.; Yang, C. M.; Waldner, P.; Zhang, H.; Fu, X. W.; Feng, X. B. Isotopic Characterization of Mercury Atmosphere-Foliage and Atmosphere-Soil Exchange in a Swiss Subalpine Coniferous Forest. *Environ. Sci. Technol.* **2023**, *57* (42), 15892−15903.
(23) Yuan, W.; Wang, X.; Lin, C. J.; Sommar, J. O.; Wang, B.; Lu, Z. Y.; Feng, X. B. Quantification of Atmospheric Mercury Deposition to and Legacy Re-emission from a Subtropical Forest Floor by Mercury Isotopes. *Environ. Sci. Technol.* **2021**, *55* (18), 12352−12361.
(24) Jiang, Z.; Cui, M.; Qian, L.; Jiang, Y.; Shi, L.; Dong, Y.; Li, J.; Wang, Y. Abiotic and biotic reduction of iodate driven by shewanella oneidensis MR-1. *Environ. Sci. Technol.* **2023**, *57* (48), 19817−19826.
(25) Wu, Y.; Zhu, X.; Wang, X.; Lin, Z.; Reinfelder, J. R.; Li, F.; Liu, T. A new electron shuttling pathway mediated by lipophilic phenoxazine via the interaction with periplasmic and inner membrane proteins of shewanella oneidensis MR-1. *Environ. Sci. Technol.* **2023**, *57* (6), 2636−2646.
(26) Zhao, C.; Duan, X.; Liu, C.; Huang, H.; Wu, M.; Zhang, X.; Chen, Y. Metabolite cross-feeding promoting nadh production and electron transfer during efficient smx biodegradation by a denitrifier and s.oneidensis MR-1 in the presence of nitrate. *Environ. Sci. Technol.* **2023**, *57* (46), 18306−18316.
(27) Lin, C. J.; Zhu, W.; Li, X. C.; Feng, X. B.; Sommar, J.; Shang, L. H. Novel dynamic flux chamber for measuring air-surface exchange of Hg-0 from soils. *Environ. Sci. Technol.* **2012**, *46*, 8910−8920.
(28) Zhang, H.; Tan, Q.; Zhang, L.; Fu, X.; Feng, X. A laboratory study on the isotopic composition of Hg(0) emitted from Hg-enriched soils in Wanshan Hg mining area. *J. Geophys. Res.: Atmos.* **2020**, *125* (19), No. e2020JD032572.
(29) Blum, J. D.; Bergquist, B. A. Reporting of variations in the natural isotopic composition of mercury. *Anal. Bioanal. Chem.* **2007**, *388*, 353−359.
(30) Liu, J.; Chen, J.; Poulain, A. J.; Pu, Q.; Hao, Z.; Meng, B.; Feng, X. Mercury and Sulfur Redox Cycling Affect Methylmercury Levels in Rice Paddy Soils across a Contamination Gradient. *Environ. Sci. Technol.* **2023**, *57* (21), 8149−8160.
(31) Fu, X.; Jiskra, M.; Yang, X.; Marusczak, N.; Enrico, M.; Chmeleff, J.; Heimbürger-Boavida, L. E.; Gheusi, F.; Sonke, J. E. Mass-Independent Fractionation of Even and Odd Mercury Isotopes during Atmospheric Mercury Redox Reactions. *Environ. Sci. Technol.* **2021**, *55*, 10164−10174.
(32) Yuan, W.; Sommar, J.; Lin, C. J.; Wang, X.; Li, K.; Liu, Y.; Zhang, H.; Lu, Z.; Wu, C.; Feng, X. Stable isotope evidence shows re-emission of elemental mercury vapor occurring after reductive loss from foliage. *Environ. Sci. Technol.* **2019**, *53* (2), 651−660.
(33) Floreani, F.; Pavoni, E.; Gosar, M.; Covelli, S. Evasion of Gaseous Elemental Mercury from Forest and Urban Soils Contaminated by Historical and Modern Ore Roasting Processes (Idrija, Slovenia). *Atmosphere* **2023**, *14* (6), 1036.
(34) García-Sánchez, A.; Contreras, F.; Adams, M.; Santos, F. Atmospheric mercury emissions from polluted gold mining areas (Venezuela). *Environ. Geochem. Health* **2006**, *28* (6), 529−540.
(35) Kocman, D.; Horvat, M. Non-point source mercury emission from the Idrija Hg-mine region: GIS mercury emission model. *J. Environ. Manage.* **2011**, *92* (8), 2038−2046.
(36) Nacht, D. M.; Gustin, M. S.; Engle, M. A.; Zehner, R. E.; Giglini, D. Atmospheric mercury emissions and speciation at the sulphur bank mercury mine superfund site, Northern California. *Environ. Sci. Technol.* **2004**, *38* (7), 1977−1983.
(37) Chen, J.; Dong, J.; Chang, J.; Guo, T.; Yang, Q.; Jia, W.; Shen, S. Characterization of an Hg (II)-volatilizing Pseudomonas sp. strain, DC-B1, and its potential for soil remediation when combined with biochar amendment. *Ecotoxicol. Environ. Saf.* **2018**, *163*, 172−179.
(38) Giovanella, P.; Cabral, L.; Costa, A. P.; de Oliveira Camargo, F. A.; Gianello, C.; Bento, F. M. Metal resistance mechanisms in Gram-negative bacteria and their potential to remove Hg in the presence of other metals. *Ecotoxicol. Environ. Saf.* **2017**, *140*, 162−169.
(39) Gustin, M. S.; Ericksen, J. A.; Schorran, D. E.; Johnson, D. W.; Lindberg, S. E.; Coleman, J. S. Application of controlled mesocosms for understanding mercury air-soil-plant exchange. *Environ. Sci. Technol.* **2004**, *38* (22), 6044−6050.

(40) Choi, H. D.; Holsen, T. M. Gaseous mercury fluxes from the forest floor of the Adirondacks. *Environ. Pollut.* **2009**, *157* (2), 592−600.
(41) Bergquist, B. A.; Blum, J. D. The odds and evens of mercury isotopes: applications of mass-dependent and mass-independent isotope fractionation. *Elements* **2009**, *5* (6), 353−357.
(42) Zheng, W.; Hintelmann, H. Isotope fractionation of mercury during its photochemical reduction by low-molecular-weight organic compounds. *J. Phys. Chem. A* **2010**, *114*, 4246−4253.
(43) Motta, L. C.; Kritee, K.; Blum, J. D.; Tsz-Ki Tsui, M.; Reinfelder, J. R. Mercury Isotope Fractionation during the Photochemical Reduction of Hg(II) Coordinated with Organic Ligands. *J. Phys. Chem. A* **2020**, *124*, 2842−2853.
(44) Sherman, L. S.; Blum, J. D.; Johnson, K. P.; Keeler, G. J.; Barres, J. A.; Douglas, T. A. Mass-independent fractionation of mercury isotopes in Arctic snow driven by sunlight. *Nat. Geosci.* **2010**, *3*, 173−177.
(45) Telahigue, K.; Rabeh, I.; Bejaoui, S.; Hajji, T.; Nechi, S.; Chelbi, E.; El Cafsi, M.; Soudani, N. Mercury disrupts redox status, up-regulates metallothionein and induces genotoxicity in respiratory tree of sea cucumber (Holothuria forskali). *Drug Chem. Toxicol.* **2020**, *43* (3), 287−297.
(46) Manceau, A.; Nagy, K. L. Thiols in Natural Organic Matter: Molecular Forms, Acidity, and Reactivity with Mercury(II) from First-Principles Calculations and High Energy-Resolution X-ray Absorption Near-Edge Structure Spectroscopy. *ACS Earth Space Chem.* **2019**, *3* (12), 2795−2807.
(47) Wang, Y.; Li, S.; Wu, X.; Zhang, J.; Feng, J.; Li, M.; Zong, S.; Yan, W. Nitrogen-Based conjugated microporous polymers for efficient Hg(II) removal from Water: Performance and mechanism. *Chem. Eng. J.* **2023**, *471*, No. 144659.
(48) Salam, L. B.; Obayori, O. S.; Ilori, M. O.; Amund, O. O. Chromium contamination accentuates changes in the microbiome and heavy metal resistome of a tropical agricultural soil. *World J. Microbiol. Biotechnol.* **2023**, *39* (9), 228.
(49) Luo, X.; Wu, C.; Lin, Y.; Li, W.; Deng, M.; Tan, J.; Xue, S. Soil heavy metal pollution from pb/zn smelting regions in china and the remediation potential of biomineralization. *J. Environ. Sci.* **2023**, *125*, 662−677.
(50) Casucci, C.; Okeke, B. C.; Frankenberger, W. T. Effects of mercury on microbial biomass and enzyme activities in soil. *Biol. Trace Elem. Res.* **2003**, *94* (2), 179−191.
(51) Thomas, J. M.; Ting, R.; Perrin, D. M. High affinity DNAzyme-based ligands for transition metal cations−a prototype sensor for $Hg^{2+}$. *Org. Biomol. Chem.* **2004**, *2* (3), 307−312.
(52) Chang, J.; Shi, Y.; Si, G.; Yang, Q.; Dong, J.; Chen, J. The bioremediation potentials and mercury(II)-resistant mechanisms of a novel fungus Penicillium spp. DC-F11 isolated from contaminated soil. *J. Hazard. Mater.* **2020**, *396*, No. 122638.
(53) Yu, Z.; Li, J.; Li, Y.; Wang, Q.; Zhai, X.; Wu, G.; Liu, P.; Li, X. A mer operon confers mercury reduction in a Staphylococcus epidermidis strain isolated from Lanzhou reach of the Yellow River. *Int. Biodeterior. Biodegrad.* **2014**, *90*, 57−63.
(54) Liang, C.; Schimel, J. P.; Jastrow, J. D. The importance of anabolism in microbial control over soil carbon storage. *Nat. Microbiol.* **2017**, *2* (8), 17105.
(55) Yin, R.; Feng, X.; Wang, J.; Li, P.; Liu, J.; Zhang, Y.; Chen, J.; Zheng, L.; Hu, T. Mercury speciation and mercury isotope fractionation during ore roasting process and their implication to source identification of downstream sediment in Wanshan mercury mining area SW China. *Chem. Geol.* **2013**, *336*, 72−79.
(56) Yin, R.; Feng, X.; Wang, J.; Bao, Z.; Yu, B.; Chen, J. Mercury isotope variations between bioavailable mercury fractions and total mercury in mercury contaminated soil in Wanshan Mercury Mine SW China. *Chem. Geol.* **2013**, *336*, 80−86.
(57) Bao, Z.; Wang, J.; Feng, X.; Shang, L. Distribution of mercury speciation in polluted soils of Wanshan mercury mining area in Guizhou. *Chin. J. Ecol.* **2011**, *30* (5), 907−913.
(58) Li, H.; Li, Y.; Tang, W.; Liu, Y.; Zheng, L.; Xu, N.; Li, Y.; Xu, D.; Gao, Y.; Zhao, J. Bioavailability and methylation of bulk mercury sulfide in paddy soils: New insights into mercury risks in rice paddies. *J. Hazard. Mater.* **2022**, *424*, No. 127394.
(59) Tian, L.; Guan, W.; Ji, Y.; He, X.; Chen, W.; Alvarez, P.; Zhang, T. Microbial methylation potential of mercury sulfide particles dictated by surface structure. *Nat. Geosci.* **2021**, *14* (6), 409−416.
(60) Konhauser, K. *Introduction to geomicrobiology*; Blackwell Publishing: Oxford, U.K., 2007.
(61) Cooper, R. E.; Eusterhues, K.; Wegner, C.; Totsche, K. U.; Küsel, K. Ferrihydrite-associated organic matter (OM) stimulates reduction by Shewanella oneidensis MR-1 and a complex microbial consortia. *Biogeosciences* **2017**, *14* (22), 5171−5188.
(62) Ravichandran, M. Interactions between mercury and dissolved organic matter−−a review. *Chemosphere* **2004**, *55* (3), 319−331.
(63) Hagele, T. J.; Mazerik, J. N.; Gregory, A.; Kaufman, B.; Magalang, U.; Kuppusamy, M. L.; Marsh, C. B.; Kuppusamy, P.; Parinandi, N. L. Mercury activates vascular endothelial cell phospholipase d through thiols and oxidative stress. *Int. J. Toxicol.* **2007**, *26* (1), 57−69.
(64) Motta, L. C.; Kritee, K.; Blum, J. D.; Tsui, M. T.; Reinfelder, J. R. Mercury Isotope Fractionation During the Photochemical Reduction of Hg(II) Coordinated With Organic Ligands. *J. Phys. Chem. A* **2020**, *124* (14), 2842−2853.
(65) Zheng, W.; Liang, L.; Gu, B. Mercury Reduction and Oxidation by Reduced Natural Organic Matter in Anoxic Environments. *Environ. Sci. Technol.* **2012**, *46*, 292−299.


https://doi.org/10.1021/acs.est.4c05220
*Environ. Sci. Technol.* 2024, 58, 16824−16832